Anomalous Hall effect in the distorted kagome magnets (Nd,Sm)Mn_6Sn_6

Wenlong Ma,[1] Xitong Xu,[2] Zihe Wang,[1] Huibin Zhou,[1] Madalynn Marshall,[3] Zhe Qu,[2,4] Weiwei Xie,[3] and Shuang Jia[1,5,6,7,*]

[1]*International Center for Quantum Materials, School of Physics, Peking University, Beijing 100871, China*
[2]*Anhui Key Laboratory of Condensed Matter Physics at Extreme Conditions, High Magnetic Field Laboratory, HFIPS, Chinese Academy of Sciences, Hefei, Anhui 230031, China*
[3]*Department of Chemistry and Chemical Biology, Rutgers University, 123 Bevier Road, Piscataway, New Jersey, 08854, USA*
[4]*CAS Key Laboratory of Photovoltaic and Energy Conservation Materials, Hefei Institutes of Physical Sciences, Chinese Academy of Sciences, Hefei, Anhui 230031, China*
[5]*Interdisciplinary Institute of Light-Element Quantum Materials and Research Center for Light-Element Advanced Materials, Peking University, Beijing 100871, China*
[6]*Collaborative Innovation Center of Quantum Matter, Beijing 100871, China*
[7]*CAS Center for Excellence in Topological Quantum Computation, University of Chinese Academy of Sciences, Beijing 100190, China*

(Received 30 March 2021; accepted 21 May 2021; published 2 June 2021)

We report magnetic and electrical properties for single crystals of $NdMn_6Sn_6$ and $SmMn_6Sn_6$. They crystallize into a structure that has distorted, Mn-based kagome lattices, compared to the pristine kagome lattices in heavy rare-earth-bearing RMn_6Sn_6 compounds. They are high-temperature ferromagnets of which the R moment is parallel with the Mn moment. We observed a large intrinsic anomalous Hall effect (AHE) that is comparable to the ferrimagnetic, heavy-R siblings in a wide range of temperature. We conclude that their intrinsic AHE is stemming from the Mn-based kagome lattice, just as in the heavy RMn_6Sn_6.

DOI: 10.1103/PhysRevB.103.235109

I. INTRODUCTION

Research on the interplay of lattice geometry, magnetic structure, electron correlation, and quantum topology is at the forefront of condensed matter physics [1–4]. Transition-metal-based kagome materials have attracted widespread attention because they often exhibit exotic quantum states including flat band [5,6], quantum spin liquid [7,8], and topological fermion [9–15]. Made of corner sharing triangles, a magnetic kagome lattice possesses strong geometrical frustration, which may induce a novel quantum topological state [16,17]. With the inclusion of spin-orbit coupling (SOC) and out-of-plane ferromagnetic (FM) ordering, a kagome lattice can effectively realize the spinless Haldane model generating Chern-gapped Dirac fermion, which renders a long-sought, high-temperature quantum anomalous Hall effect (QAHE) [3,18,19]. However, pristine kagome lattices with strong out-of-plane magnetization are scarce in binary transition-metal compounds.

A family of RMn_6Sn_6 (R = heavy rare-earth element) compounds, crystallizing into a $HfFe_6Ge_6$-type structure ($P6/mmm$), host a pristine Mn-based kagome lattice, which generates various quantum magnetic properties [21–26]. The R elements play an important role on the structural and magnetic properties of RMn_6Sn_6 [27–29]. The $HfFe_6Ge_6$-type structure can be viewed as a R-stuffed CoSn-type structure [Figs. 1(a)–1(c)] [20,30]. Caged in the polyhedron made by Mn kagome and Sn honeycomb nets, the R elements push the Sn sites at the top and bottom of the void space away from the hexagonal center of the kagome net [Fig. 1(b)]. This arrangement leads to an alternation of stuffed and empty cavities along the c axis, which forms a layered structure [Fig. 1(c)]. The pristine Mn-based kagome layer and the weak interlayer coupling in this layered structure are believed to facilitate the electron hopping in the kagome sites, which is crucial to realize the topological electron band [22].

It is well-known that the spin parts of the $4f$ and $3d$ moments are prone to be coupled antiparallel in many rare-earth transition metal intermetallics [31,32]. Therefore the total moment of the Hund's ground state of the heavy R is coupled antiparallel to the transition metal moment whereas it is reverse for the light R. Just as observed in heavy RMn_6Sn_6 compounds, the magnetic R sublattice tends to develop an antiparallel configuration with respect to the FM ordered Mn lattice [28,29]. Strong antiparallel magnetic coupling between the anisotropic R moments and Mn moments leads to a ferrimagnetic (FIM) state in the RMn_6Sn_6 family (R = Gd - Er). In particular, $TbMn_6Sn_6$, consisting of a high-temperature, out-of-plane FM ordered Mn-based kagome lattice, was discovered to be a near-ideal quantum-limit magnet with Chern-gapped, massive Dirac fermion [22]. Very recently we found the massive Dirac fermion generally exists in the FM Mn-based kagome lattices in RMn_6Sn_6 for R = Gd - Er [21], whose Berry curvature field generates a large intrinsic anomalous Hall effect (AHE). For comparison, the isostructural (Y, Lu)Mn_6Sn_6 with nonmagnetic R atoms show a flat spiral antiferromagnetic (AFM) ordering of Mn moment

*gwljiashuang@pku.edu.cn

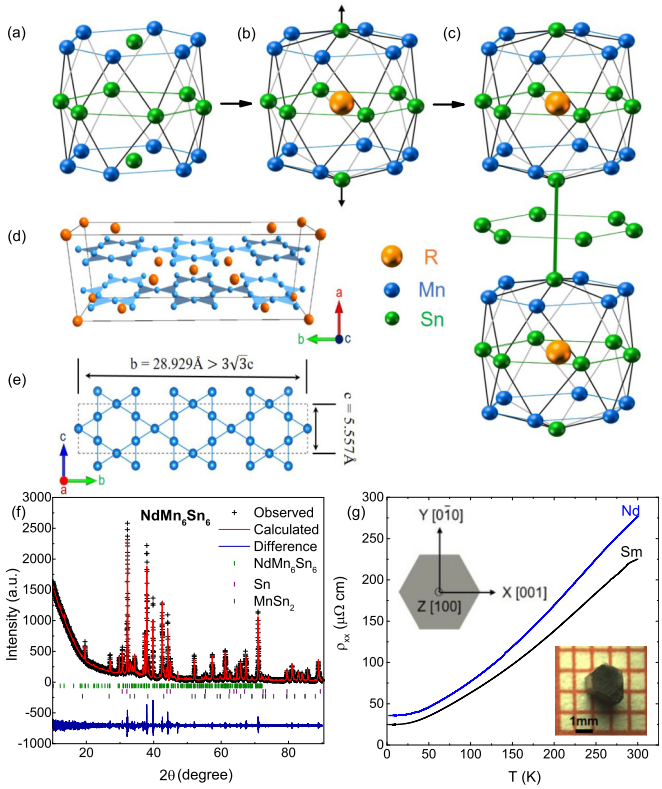

FIG. 1. Crystal structure and resistivity of (Nd, Sm)Mn_6Sn_6. (a) to (c) describe the formation of RMn_6Sn_6 structure by stuffing an R ion into a CoSn-type structure. (a) An empty polyhedron in the CoSn-type structure. (b) R ion is stuffed into the polyhedron forming a pristine kagome lattice. (c) A layered RMn_6Sn_6 structure is formed [20]. (d) Distorted Mn-based kagome layers and R atoms in a unit cell of (Nd, Sm)Mn_6Sn_6. R atoms: yellow; Mn atoms: blue. (e) The distorted Mn-based kagome layer. (f) Refined powder XRD pattern of $NdMn_6Sn_6$. (g) Temperature dependence of in-plane, zero-field longitudinal resistivity. Top inset: Sketch of the crystallographic orientations. Bottom inset: Photo of a single crystal of $NdMn_6Sn_6$ on 1-mm grid paper.

[33,34]. A large topological Hall effect (THE) was observed in YMn_6Sn_6 [23,25].

In this paper we focus on (Nd, Sm)Mn_6Sn_6, two light rare-earth siblings that have not been synthesized in a single-crystalline form until now, as far as we are aware. Previous studies on its polycrystalline form showed several unique structural and magnetic properties unlike those in the heavy RMn_6Sn_6. They crystallize into the $HoFe_6Sn_6$-type structure (*Immm*), another R-stuffed CoSn-type structure. Unlike the $HfFe_6Ge_6$-type structure in which the R-stuffed polyhedron stacks along the *c* axis in hexagonal cells, here the polyhedron forms triple rows along the *c* axis and stacking along the *a* axis in orthorhombic unit cells [Fig. 1(d)]. The triple rows of stuffed and empty cavities are alternatively arranged along the *b* axis, leading to a larger unit cell which has a relation with the hexagonal cell as $a_o = c_h$, $b_o = 3\sqrt{3}a_h$, and $c_o = b_h$ [Fig. 1(d)] [20,30]. The structure distortion not only stretches the Mn kagome lattice along the *b* axis, but also wrinkles it very slightly in the *a* plane because the Mn atoms have four different crystallographic sites and coordinations now [Fig. 1(e)]. The magnetic coupling between the light R and Mn moment is parallel in (Nd, Sm)Mn_6Sn_6, leading to a collinear FM ordering above room temperature [35]. Neutron diffraction on the polycrystalline samples show $SmMn_6Sn_6$ is an easy-plane ferromagnet with the Curie temperature T_C = 405 K, while $NdMn_6Sn_6$ undergoes two spin-reorientation transitions below its T_C = 357 K [35].

We investigate the magnetic anisotropy in single-crystalline (Nd, Sm)Mn_6Sn_6 and confirm the previously determined crystalline and magnetic structure in the polycrystals [35,36]. In general they are soft ferromagnets with a large saturated magnetic moment consisting of parallel R and Mn moments. In particular, $NdMn_6Sn_6$ contains a distorted Mn-based kagome lattice with out-of-plane magnetization, similar to $TbMn_6Sn_6$. (Nd, Sm)Mn_6Sn_6 possess a large intrinsic anomalous Hall conductivity (AHC) $\sigma_{AH}^{int} \sim 100 - 200\,\Omega^{-1}\,cm^{-1}$ below room temperature, which is comparable to the intrinsic AHC in FIM heavy RMn_6Sn_6 [21]. Comparing the AHE in (Nd, Sm)Mn_6Sn_6 to that in heavy RMn_6Sn_6, we prove that the intrinsic AHE is stemming from the Mn lattice, while the scattering effect of R moments seems to be irrelevant.

II. EXPERIMENTAL RESULTS

Single crystals of (Nd, Sm)Mn_6Sn_6 were synthesized by a tin-flux method [29,37]. The details of the crystal growth and experimental methods can be found in Sec. I of the Supplemental Material [38]. Powder x-ray diffraction (PXRD) data collected on pulverized $NdMn_6Sn_6$ [Fig. 1(f)] was refined in the $HoFe_6Sn_6$-type structure plus a tiny amount of Sn and $MnSn_2$ impurities. The PXRD pattern for $SmMn_6Sn_6$ shows two structures ($HoFe_6Sn_6$ and $HfFe_6Ge_6$-type) of crystals (Fig. S1 within the Supplemental Material [38]). The result is consistent with the work on the polycrystal by Malaman *et al.* [35] who reported that $SmMn_6Sn_6$ crystalizes into two structures at different synthesis temperatures. We cannot distinguish the different structural crystals by appearance, however, the magnetization and transport measurements on several pieces show no explicit difference. Therefore, we use the $HoFe_6Sn_6$-type structure to describe the sample below.

The typical sample morphology is a hexagonal prism [bottom inset of Fig. 1(g)] whose hexagonal surface is confirmed

TABLE I. Summary of the refined lattice parameters of the (Nd, Sm)Mn_6Sn_6 single crystals.

R	Space group	*Z*	*a*(Å)	*b*(Å)	*c*(Å)	*V*(Å^3)
Nd	*Immm*	6	9.0616(3)	28.9291(8)	5.5575(2)	1456.8650(5)
Sm (Phase1)	*Immm*	6	9.0649(5)	28.9581(16)	5.5870(3)	1466.6002(8)
Sm (Phase2)	*P*6/*mmm*	1	5.5487(1)	5.5487(1)	9.0438(2)	241.1340(3)

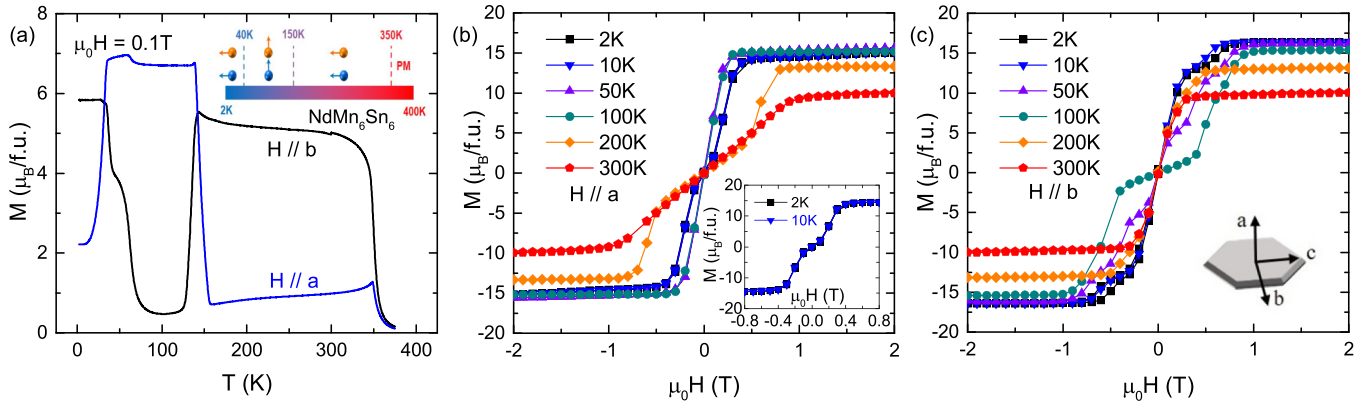

FIG. 2. Magnetization (M) of $NdMn_6Sn_6$. (a) Temperature dependence of M with an external magnetic field ($\mu_0 H = 0.1$ T) along crystallographic a and b directions. Inset: Magnetic structures in zero field at different temperatures. The blue and yellow spheres with arrows represent the Mn and Nd magnetic moments along different directions, respectively. (b) $M(H)$ curves at different temperatures when H is applied along the a axis. Inset shows the zoom-in $M(H)$ profiles at 2 and 10 K. (c) $M(H)$ curves at different temperatures when H is applied along the b axis. Inset shows the crystallographic orientations.

to be the (100) plane by a Laue diffraction. The crystallographic orientations are shown in the upper inset of Fig. 1(g). As shown in Table I and Fig. 1(e), the ratio of lattice constants b and c for $NdMn_6Sn_6$ is slightly larger than $3\sqrt{3}$, reflecting the stretch of its kagome lattice. It is noteworthy that the lattice parameters of $SmMn_6Sn_6$ are slightly larger than those of $NdMn_6Sn_6$. Violation of the lanthanide contraction may indicate an unstable valence of Sm ions.

Temperature dependent, zero-field longitudinal resistivity $\rho_{xx}(T)$ of (Nd, Sm)Mn_6Sn_6 is presented in Fig. 1(g) when the current (I) is applied along the c axis. Their residual resistivity ratio [$RRR = \rho(300\text{K})/\rho(2\text{K})$] is around 10. Because the resistivity ρ_{zz} for $I \parallel a$ is close to ρ_{xx} at room temperature, we use an isotropic ρ_{xx} to analysis the data below.

A uniaxial anisotropy is observed in the magnetization curves $M(H)$ when H is along three crystallographic orientations. While the $M(H)$ curves for $H \parallel b$ and c directions are identical (the latter is shown in Fig. S3 within the Supplemental Material [38]), the anisotropic magnetic properties are demonstrated when H is applied along the a and b directions (shown in Figs. 2 and 3). On the whole our results are consistent with that of the magnetization and neutron scattering experiments on the polycrystals [35]. Below we show the details of single crystals that were unresolved before.

According to the $M(T)$ curves, $NdMn_6Sn_6$ has an FM transition with a T_C of about 350 K, similar to 357 K observed for the polycrystal [35] [Fig. 2(a)]. Below the T_C, the $M(T)$ curves show two sharp spin-reorientation transitions in which the easy axis changes from in-plane to out-of-plane at about 150 K and then back to in-plane at about 40 K [Fig. 2(a) and inset]. These complicated spin-reorientation transitions were also detected in neutron scattering [35]. Yet we observed some peculiar features on the $M(T)$ curves between 60 and 40 K, which may be stemming from some unknown magnetic structure changes.

The spin-reorientation transitions are visible in a series of $M(H)$ curves when H is along the a and b axes [Figs. 2(b) and 2(c)]. Overall the single crystal of $NdMn_6Sn_6$ is a soft magnet whose magnetization is saturated in a small field ($\mu_0 H < 1$ T) along all directions below room temperature. The saturated

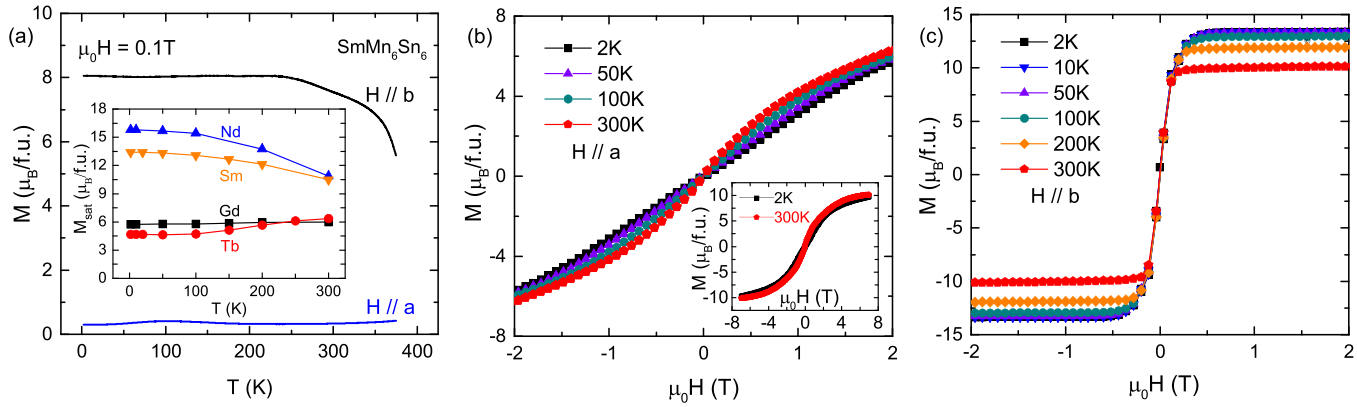

FIG. 3. Magnetization (M) of $SmMn_6Sn_6$. (a) Temperature dependence of M with an external magnetic field ($\mu_0 H = 0.1$ T) along crystallographic a and b directions. Inset: Temperature dependence of the saturated magnetization (M_{sat}) for (Nd, Sm)Mn_6Sn_6 and (Gd, Tb)Mn_6Sn_6. (b) $M(H)$ curves at different temperatures when H is applied along the a axis. Inset shows the whole profiles at 2 and 300 K. (c) $M(H)$ curves at different temperatures when H is applied along the b axis.

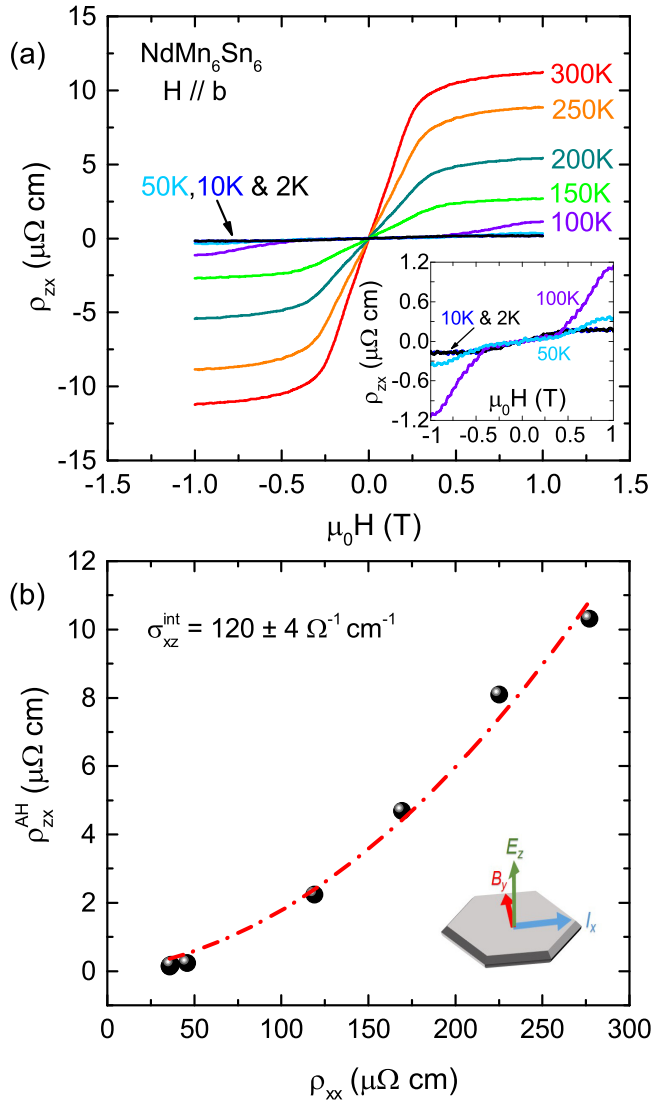

FIG. 4. AHE of $NdMn_6Sn_6$ when the external magnetic field is applied along the b axis. (a) Field dependence of ρ_{zx} at different temperatures. Inset: Zoom-in plot at low temperatures. (b) ρ_{zx}^{AH} plotted against ρ_{xx} from 2 K to 300 K. The red dashed line represents the polynomial fitting of the data points ($\rho_{AH} = \sigma^{\text{int}}\rho_{xx}^2 + \alpha^{\text{skew}}\rho_{xx}$), which gives the intrinsic anomalous Hall conductivity σ_{xz}^{int}. The bottom inset illustrates the geometry of the Hall measurement.

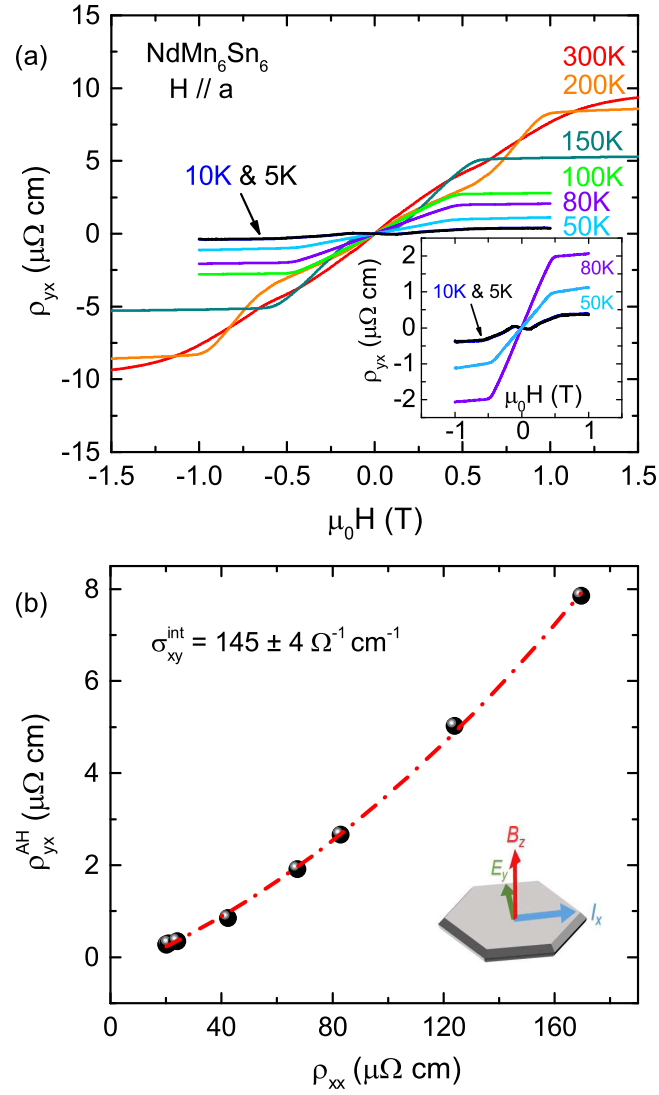

FIG. 5. AHE of $NdMn_6Sn_6$ when the external magnetic field is applied along the a axis. (a) Field dependence of ρ_{yx} at different temperatures. Inset: Zoom-in plot at at low temperatures. (b) ρ_{yx}^{AH} plotted against ρ_{xx} from 5 K to 300 K. σ_{xy}^{int} is given by the polynomial fitting of the data points (red dashed line). The bottom inset illustrates the geometry of the Hall measurement.

magnetization (M_{sat}) is about 15 μ_B/f.u. at 2 K, which is constituent of six Mn moments and one Nd moment in parallel [Fig. 2(b)]. M_{sat} gradually decreases to 10 μ_B/f.u. as the temperature increases to 300 K. An external field less than 0.4 T along the hard direction drives the spin-reorientation when the temperature is below 40 K [inset of Fig. 2(b)]. At higher temperature the spin-reorientation requires a slightly larger external field, no more than 1 T at 300 K.

The magnetic structure of $SmMn_6Sn_6$ is rather simple as we observed an easy-plane FM state in the $M(T)$ curves for the whole temperature range [Fig. 3(a)]. Its T_C was reported to be about 400 K [35,36], which is beyond our measurement range. When the field is applied in-plane, the $M(H)$ curves show a typical soft FM profile and the M_{sat} is about 13 μ_B/f.u. at 2 K and gradually decreases to 10 μ_B/f.u. at 300 K [Fig. 3(c)]. In an out-of-plane magnetic field, M steadily increases and shows no trend of saturation at 7 T [Fig. 3(b) and inset].

We compare the M_{sat} of (Nd, Sm)Mn_6Sn_6 and (Gd, Tb)Mn_6Sn_6, which have easy-plane and easy-axis FIM states below their T_C, respectively. The M_{sat} of (Gd, Tb)Mn_6Sn_6 gradually increases from 5.7 and 4.6 μ_B/f.u. at 2 K to 6.0 and 6.4 μ_B/f.u. at 300 K, respectively [inset of Fig. 3(a)]. If we assume the saturated moments of the R^{3+} take the values of their Hund's rule ground states at 2 K (7 and 9 μ_B/f.u. for Gd^{3+} and Tb^{3+}, respectively), then we derive that the saturated moment of one Mn atom equals 2.1 and 2.3 μ_B, respectively. This result is comparable to the values in previous work [39]. Then we estimate the saturated moment of one Mn atom at 2 K for (Nd, Sm)Mn_6Sn_6 in the same way, which is about 2.0 and 2.1 μ_B, respectively. The opposite trend of the M_{sat} with the

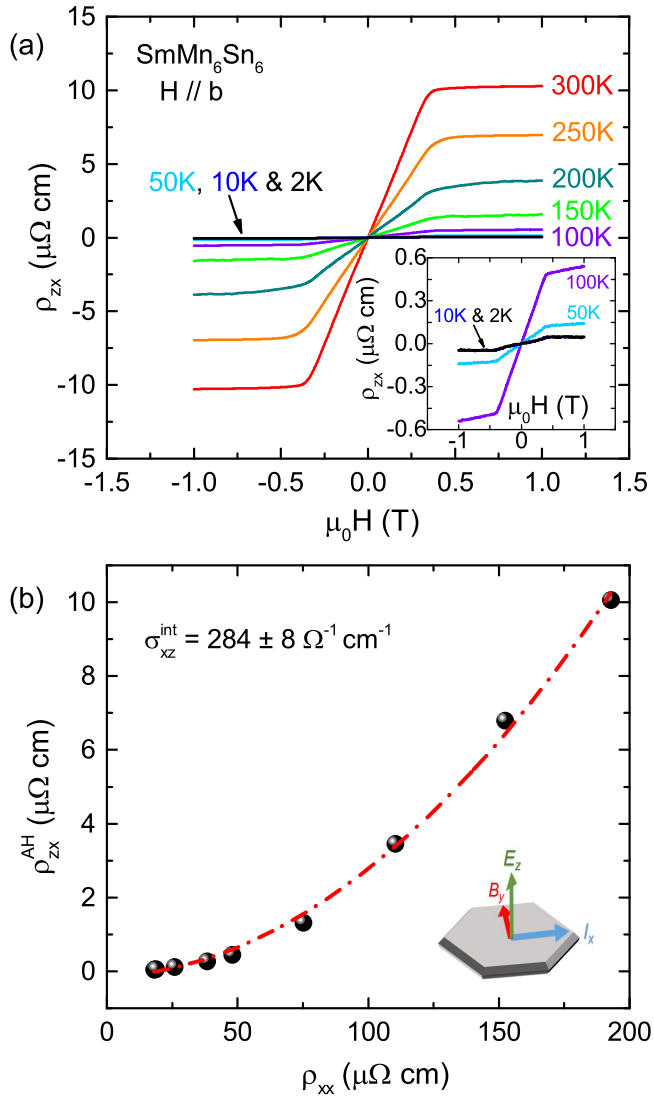

FIG. 6. AHE of $SmMn_6Sn_6$ when the external magnetic field is applied along the b axis. (a) Field dependence of ρ_{zx} at different temperatures. Inset: Zoom-in plot at low temperatures. (b) ρ_{zx}^{AH} plotted against ρ_{xx} from 2 K to 300 K. σ_{xz}^{int} is given by the polynomial fitting of the data points (red dashed line). The bottom inset illustrates the geometry of the Hall measurement.

temperature change for light and heavy R indicates that the M_{sat} change in temperature is mainly due to the damping of the rare-earth moment with increasing temperature.

Given the fast-saturating $M(H)$ curves, we speculate that the AHE can be easily detected in $NdMn_6Sn_6$ when a weak magnetic field is applied along any direction, but can only be detected in $SmMn_6Sn_6$ when a weak magnetic field is applied in-plane. Unfortunately, we found that the crystals are prone to crack under a magnetic field higher than 1 T, which might be due to a large magnetostriction effect. However, note that we did not meet this difficulty when measuring the heavy R siblings. Figures 4–6 show the Hall resistivity, ρ_{zx} when $H \parallel b$, and ρ_{yx} when $H \parallel a$ for $NdMn_6Sn_6$ and ρ_{zx} for $SmMn_6Sn_6$ at different temperatures, respectively. To avoid the sample damage we restricted the external field to less than 1.5 T.

The ρ_{zx} and ρ_{yx} of $NdMn_6Sn_6$ follow the $M(H)$ isotherms in the whole temperature range, showing a large AHE above 100 K [Figs. 4(a) and 5(a)]. The spin-reorientation transitions drive relevant changes in the ρ_{zx} and ρ_{yx} curves at various temperatures. It is noteworthy that the ρ_{yx} curves below 10 K are peculiar in weak field: They show a negative initial slope and a hump at about 0.1 T [inset of Fig. 5(a)], which is seemingly related to the spin-reorientation process at low temperatures [inset of Fig. 2(b)]. The reason for the negative initial slope in ρ_{yx} below 10 K is still not clear. In a stronger field ρ_{yx} changes sign and is prone to saturate when $\mu_0 H > 0.5$ T corresponding to the saturating external field of M. The ρ_{zx} of $SmMn_6Sn_6$ roughly resembles the $M(H)$ curves as well [Fig. 6(a)].

III. ANALYSIS AND DISCUSSION

Except for the peculiar feature mentioned above in $NdMn_6Sn_6$ below 10 K, the Hall resistivity can be related to the magnetization as described by the following equation [40]:

$$\rho_{yx} = \rho_{OH}(B) + \rho_{AH}(M) = R_0 B + R_S 4\pi M, \quad (1)$$

where B is the magnetic induction field, ρ_{OH} and ρ_{AH} are the ordinary and anomalous Hall resistivity, R_0 and R_S are the ordinary and anomalous Hall coefficients, respectively.

The AHE is known to have origins from intrinsic and extrinsic (skew-scattering and side-jump while the later is usually small) mechanisms [40]. Since M_{sat}(T) changes small over the temperature range we investigate [M_{sat}(300K)/M_{sat}(2K) $\sim$ 0.7], we ignore the effect of the M_{sat} change on the AHE [41,42]. In order to untangle the intrinsic term, we use the following equation [41]:

$$\rho_{AH} = \sigma^{int}\rho_{xx}^2 + \alpha^{skew}\rho_{xx}, \quad (2)$$

where σ^{int} is the intrinsic AHC and α^{skew} is the skew-scattering contribution parameter. Using a standard polynomial fitting, we obtained σ^{int} as about 130 Ω^{-1} cm^{-1} for two directions in $NdMn_6Sn_6$ and about 284 Ω^{-1} cm^{-1} in $SmMn_6Sn_6$ [Figs. 4(b) to 6(b)]. The similar values of σ^{int} can be obtained by using a modified Tian-Ye-Jin scaling method [43]. The values of α^{skew} for (Nd, Sm)Mn_6Sn_6 have the same magnitude of order as that for FIM heavy RMn_6Sn_6 ($\sim 5 \times 10^{-3}$) [21].

Comparing ρ_{AH} and σ_{xy}^{int} in $NdMn_6Sn_6$ to that in $TbMn_6Sn_6$, we find they have the same sign and are close in magnitude, albeit the M_{sat} of $NdMn_6Sn_6$ in the FM state is several times larger than that of $TbMn_6Sn_6$ in FIM state. This observation can be well understood if the AHE is mainly stemming from the Mn lattice while the scattering effect of R moments is negligible. The σ_{xy}^{int} in $NdMn_6Sn_6$ corresponds to $(0.17 \pm 0.01)\, e^2/h$ per kagome layer, close to the value of $TbMn_6Sn_6$ as well [22]. Comparing their crystal structures, we notice the Sn and R atoms have been rearranged while the Mn kagome lattice only has a slight distortion. We speculate that the crystal structure change does not significantly modify the Berry curvature field. It needs further study to clarify whether and how the structural distortion impacts the massive Dirac fermion which was hosted in the Mn kagome lattice.

Another interesting observation is that $SmMn_6Sn_6$ seems to have a larger σ_{xz}^{int} compared to that of $GdMn_6Sn_6$, which has an easy-plane FIM state [44]. A plausible valance instability of the Sm ion may affect its electron structure. The effect of

the R valence instability on the topological electron properties of the RMn_6Sn_6, including $SmMn_6Sn_6$ and $YbMn_6Sn_6$, needs further elaboration.

IV. CONCLUSIONS

In summary, we investigate the magnetic and electrical properties of single-crystalline (Nd, Sm)Mn_6Sn_6 whose crystal structure features distorted Mn kagome lattices. The compounds are soft, room-temperature ferromagnets with an easy-plane or easy-axis anisotropy with respect to the kagome plane. They possess a large intrinsic AHE comparable to that in the FIM heavy RMn_6Sn_6. Their intrinsic AHE is stemming from the Berry curvature field in Mn-based kagome lattice as well.

The kagome magnets are candidates for quantum materials, but the distorted kagome magnets were rarely studied. Our observation demonstrates a large, Berry curvature field induced AHE in distorted kagome magnets. Noticing that a large family of RT_6X_6 (T = transition metal, X = metalloid) compounds crystallize into various structures consisting of distorted and pristine T-based kagome lattices [45–50], their topological properties and the relationship with their lattice geometry and magnetic structures are worth investigating.

ACKNOWLEDGMENTS

We would like to thank Prof. Yuan Li for using their wire cutting machine, Dr. Jia-Xin Yin for helpful discussions. This work was supported by the National Natural Science Foundation of China Grants No. U1832214, No. 11774007, No. U2032213, No. 11774352, the National Key R&D Program of China (2018YFA0305601) and the strategic Priority Research Program of Chinese Academy of Sciences, Grant No. XDB28000000. X.X. acknowledges support from the China Postdoctoral Science Foundation Grant No. 2020M682056 and Anhui Postdoctoral Foundation Grant No. 2020B472. X.X. is also supported by the HFIPS Director's Fund, Grant No. YZJJ2021QN28 and Special Research Assistant, Chinese Academy of Sciences. The work at Rutgers is supported by Beckman Young Investigator Award.

[1] B. Keimer and J. Moore, Nat. Phys. **13**, 1045 (2017).
[2] Y. Tokura, K. Yasuda, and A. Tsukazaki, Nat. Rev. Phys. **1**, 126 (2019).
[3] F. D. M. Haldane, Phys. Rev. Lett. **61**, 2015 (1988).
[4] C.-Z. Chang, J. Zhang, X. Feng, J. Shen, Z. Zhang, M. Guo, K. Li, Y. Ou, P. Wei, L.-L. Wang *et al.*, Science **340**, 167 (2013).
[5] J.-X. Yin, S. S. Zhang, G. Chang, Q. Wang, S. S. Tsirkin, Z. Guguchia, B. Lian, H. Zhou, K. Jiang, I. Belopolski *et al.*, Nat. Phys. **15**, 443 (2019).
[6] M. Kang, L. Ye, S. Fang, J.-S. You, A. Levitan, M. Han, J. I. Facio, C. Jozwiak, A. Bostwick, E. Rotenberg *et al.*, Nat. Mater. **19**, 163 (2020).
[7] J. S. Helton, K. Matan, M. P. Shores, E. A. Nytko, B. M. Bartlett, Y. Yoshida, Y. Takano, A. Suslov, Y. Qiu, J.-H. Chung, D. G. Nocera, and Y. S. Lee, Phys. Rev. Lett. **98**, 107204 (2007).
[8] T.-H. Han, J. S. Helton, S. Chu, D. G. Nocera, J. A. Rodriguez-Rivera, C. Broholm, and Y. S. Lee, Nature **492**, 406 (2012).
[9] S. Nakatsuji, N. Kiyohara, and T. Higo, Nature **527**, 212 (2015).
[10] K. Kuroda, T. Tomita, M.-T. Suzuki, C. Bareille, A. Nugroho, P. Goswami, M. Ochi, M. Ikhlas, M. Nakayama, S. Akebi *et al.*, Nat. Mater. **16**, 1090 (2017).
[11] E. Liu, Y. Sun, N. Kumar, L. Muechler, A. Sun, L. Jiao, S.-Y. Yang, D. Liu, A. Liang, Q. Xu *et al.*, Nat. Phys. **14**, 1125 (2018).
[12] L. Ye, M. Kang, J. Liu, F. Von Cube, C. R. Wicker, T. Suzuki, C. Jozwiak, A. Bostwick, E. Rotenberg, D. C. Bell *et al.*, Nature **555**, 638 (2018).
[13] J.-X. Yin, S. S. Zhang, H. Li, K. Jiang, G. Chang, B. Zhang, B. Lian, C. Xiang, I. Belopolski, H. Zheng *et al.*, Nature **562**, 91 (2018).
[14] D. Liu, A. Liang, E. Liu, Q. Xu, Y. Li, C. Chen, D. Pei, W. Shi, S. Mo, P. Dudin *et al.*, Science **365**, 1282 (2019).
[15] N. Morali, R. Batabyal, P. K. Nag, E. Liu, Q. Xu, Y. Sun, B. Yan, C. Felser, N. Avraham, and H. Beidenkopf, Science **365**, 1286 (2019).
[16] K. Ohgushi, S. Murakami, and N. Nagaosa, Phys. Rev. B **62**, R6065 (2000).
[17] N. J. Ghimire and I. I. Mazin, Nat. Mater. **19**, 137 (2020).
[18] E. Tang, J.-W. Mei, and X.-G. Wen, Phys. Rev. Lett. **106**, 236802 (2011).
[19] G. Xu, B. Lian, and S.-C. Zhang, Phys. Rev. Lett. **115**, 186802 (2015).
[20] D. C. Fredrickson, S. Lidin, G. Venturini, B. Malaman, and J. Christensen, J. Am. Chem. Soc. **130**, 8195 (2008).
[21] W. Ma, X. Xu, J.-X. Yin, H. Yang, H. Zhou, Z.-J. Cheng, Y. Huang, Z. Qu, F. Wang, M. Z. Hasan, and S. Jia, arXiv:2007.09913.
[22] J.-X. Yin, W. Ma, T. A. Cochran, X. Xu, S. S. Zhang, H.-J. Tien, N. Shumiya, G. Cheng, K. Jiang, B. Lian *et al.*, Nature **583**, 533 (2020).
[23] N. J. Ghimire, R. L. Dally, L. Poudel, D. Jones, D. Michel, N. T. Magar, M. Bleuel, M. A. McGuire, J. Jiang, J. Mitchell *et al.*, Sci. Adv. **6**, eabe2680 (2020).
[24] H. Zhang, X. Feng, T. Heitmann, A. I. Kolesnikov, M. B. Stone, Y.-M. Lu, and X. Ke, Phys. Rev. B **101**, 100405(R) (2020).
[25] Q. Wang, K. J. Neubauer, C. Duan, Q. Yin, S. Fujitsu, H. Hosono, F. Ye, R. Zhang, S. Chi, K. Krycka, H. Lei, and P. Dai, Phys. Rev. B **103**, 014416 (2021).
[26] C. M. III, W. Ma, V. Pomjakushin, O. Zaharko, X. Liu, J. X. Yin, S. S. Tsirkin, T. A. Cochran, M. Medarde, V. Poree, D. Das, C. N. Wang, J. Chang, T. Neupert, A. Amato, S. Jia, M. Z. Hasan, H. Luetkens, and Z. Guguchia, arXiv:2101.05763.
[27] G. Venturini, B. E. Idrissi, and B. Malaman, J. Magn. Magn. Mater. **94**, 35 (1991).
[28] B. Malaman, G. Venturini, R. Welter, J. Sanchez, P. Vulliet, and E. Ressouche, J. Magn. Magn. Mater. **202**, 519 (1999).
[29] D. Clatterbuck and K. Gschneidner, J. Magn. Magn. Mater. **207**, 78 (1999).
[30] G. Venturini, Z. Kristallogr. Cryst. Mater. **221**, 511 (2006).
[31] S. Sinnema, R. Radwanski, J. Franse, D. De Mooij, and K. Buschow, J. Magn. Magn. Mater. **44**, 333 (1984).

[32] M. Brooks, L. Nordström, and B. Johansson, Phys. B **172**, 95 (1991).
[33] R. L. Dally, J. W. Lynn, N. J. Ghimire, D. Michel, P. Siegfried, and I. I. Mazin, Phys. Rev. B **103**, 094413 (2021).
[34] G. Venturini, R. Welter, B. Malaman, and E. Ressouche, J. Alloy. Compd. **200**, 51 (1993).
[35] B. Malaman, G. Venturini, B. C. El Idrissi, and E. Ressouche, J. Alloy. Compd. **252**, 41 (1997).
[36] F. Weitzer, A. Leithe-Jasper, K. Hiebl, P. Rogl, Q. Qi, and J. Coey, J. Appl. Phys **73**, 8447 (1993).
[37] P. C. Canfield and Z. Fisk, Philos. Mag. B **65**, 1117 (1992).
[38] See Supplemental Material at http://link.aps.org/supplemental/10.1103/PhysRevB.103.235109 for experimental details as well as additional figures and discussions.
[39] L. Zhang, Ph.D. thesis, Universiteit van Amsterdam, 2005.
[40] N. Nagaosa, J. Sinova, S. Onoda, A. H. MacDonald, and N. P. Ong, Rev. Mod. Phys. **82**, 1539 (2010).
[41] C. Zeng, Y. Yao, Q. Niu, and H. H. Weitering, Phys. Rev. Lett. **96**, 037204 (2006).
[42] B. C. Sales, R. Jin, D. Mandrus, and P. Khalifah, Phys. Rev. B **73**, 224435 (2006).
[43] Y. Tian, L. Ye, and X. Jin, Phys. Rev. Lett. **103**, 087206 (2009).
[44] T. Asaba, S. M. Thomas, M. Curtis, J. D. Thompson, E. D. Bauer, and F. Ronning, Phys. Rev. B **101**, 174415 (2020).
[45] P. Schobinger-Papamantellos, J. Rodríguez-Carvajal, and K. Buschow, J. Alloy. Compd. **256**, 92 (1997).
[46] J. Brabers, K. Buschow, and F. De Boer, J. Alloy. Compd. **205**, 77 (1994).
[47] G. Venturini, R. Welter, and B. Malaman, J. Alloy. Compd. **185**, 99 (1992).
[48] X.-L. Rao and J. Coey, J. Appl. Phys **81**, 5181 (1997).
[49] T. Mazet and B. Malaman, J. Alloy. Compd. **325**, 67 (2001).
[50] A. Szytuła, E. Wawrzyńska, and A. Zygmunt, J. Alloy. Compd. **366**, L16 (2004).